TURBO Vol. 15 No. 2. 2026
Jurnal Program Studi Teknik Mesin UM Metro
p-ISSN: 2301-6663, e-ISSN: 2477-250X
URL: http://ojs.ummetro.ac.id/index.php/turbo

Kinetic Profile of CO and CO_2 Formation in PET Catalytic Pyrolysis Using Local Biomass-Based Functional Carbon Materials

Asriwulan[1*], Ahmad Yani[2*], Muh. Awalul Agus[3], Fitria[4], Ratnawati[5], Anita Sardewi[6], Slamet Hariyadi[7]
[1,3,4,6]Prodi Teknik Kimia, Sekolah Tinggi Teknologi Industri Bontang
[2,5,7]Prodi Teknik Mesin, Sekolah Tinggi Teknologi Industri Bontang
Jl. Brigjend Katamso No.40, Kota Bontang, Kalimantan Timur, Indonesia
**Corresponding author*: asriwulan45@gmail.com; yanibima@gmail.com

Abstract

This study evaluated the kinetic profile of CO and CO_2 gas formation during Polyethylene Terephthalate (PET) pyrolysis at 350°C with the addition of local biomass-based functional carbon materials, namely hibiscus flower powder (Hibiscus rosa-sinensis/HRS), ulin wood activated carbon (Eusideroxylon zwageri Activated Carbon/EZAC), and their mixture (1:1). Pyrolysis was carried out in a stainless-steel batch fixed-bed reactor with an in-situ configuration under a 5 wt% catalyst loading (PET-to-catalyst ratio of 95:5). The non-condensable gaseous products were continuously monitored via a real-time measurement method integrated with MQ-7 and MQ-135 semiconductor sensors.The results showed that catalyst addition accelerated the onset of gas formation compared with neat PET (CO onset at 1601 s; CO_2 onset at 1672 s). EZAC outperformed the other samples across all CO kinetic parameters (onset at 203 s, rate of 0.696 ppm/s, peak concentration of 927 ppm), whereas HRS outperformed the other samples in the CO_2 formation rate (0.294 ppm/s, peak concentration of 600 ppm), indicating distinct mechanistic roles for the two materials. HRS selectively promoted decarboxylation, supported by its potassium (K) content and amorphous structure, whereas EZAC selectively promoted decarbonylation owing to its oxygen-containing functional groups and disordered carbon structure. FTIR, SEM-EDX, XRD, and TGA-DTA characterization supported this mechanistic interpretation, demonstrating that combining raw biomass with activated carbon successfully tailors the kinetic evolution of gaseous products, which serves as a practical approach for selectively controlling gas emissions in plastic waste valorization.

Keywords: *activated carbon, carbon monoxide and carbon dioxide formation, functional carbon material, plastic waste pyrolysis, reaction kinetics*.

1. Introduction

The development of local biomass-based functional carbon materials has become one of the strategies for sustainable waste valorization, particularly for catalytic applications. Polyethylene Terephthalate (PET) is among the most widely produced and consumed plastics globally, contributing significantly to the accumulation of plastic waste that is not readily biodegradable [1]. Pyrolysis is a chemical recycling approach capable of converting PET waste into gas, liquid (oil), and solid (char) products that can be reused. During pyrolysis, thermal degradation breaks the ester chains in PET, generating oxygenated intermediates that subsequently undergo decarboxylation and decarbonylation reactions, producing CO and CO_2 as the two major gaseous products [2]. Studies on PET pyrolysis have shown that CO_2 is formed through decarboxylation during the early stage of degradation, whereas CO is formed through radical decarbonylation during the secondary stage of degradation [3]. The character of these two reaction pathways is reflected not only in the amount of gas formed but also in the timing of their appearance and their formation rate.

Catalyst addition has been widely reported to modify these reaction pathways. Alkali and alkaline earth metals (AAEM) contained in biomass are known to act as natural catalysts, accelerating the initial stage of decomposition and affecting the cleavage of carboxyl and carbonyl groups, thereby promoting the decarboxylation reaction [4,5]. On the other hand, carbonized wood biomass converted into activated

DOI: https://doi.org/10.24127/trb.v15i2.5557
Received 1 September 2026; Received in revised form 2 November 2026; Accepted 4 November 2026
Available online 1 December 2026

carbon possesses a high surface area and diverse oxygen-containing functional groups on its surface that play a key role in catalytic activity and selectivity [6], acting as a catalytic support material that provides contact space between volatile compounds and the reactive sites of the activated carbon, supporting secondary cracking and decarbonylation reactions [7].

The utilization of biomass-waste-based carbon materials as plastic pyrolysis catalysts is also in line with the circular economy principle that promotes resource efficiency [8]. Separate physicochemical characterization studies of hibiscus flower powder (HRS) and ulin wood activated carbon (EZAC) have reported that both materials have potential for use as catalysts in PET pyrolysis [9]. A study on the co-pyrolysis of PET with HRS showed an increase in gas production compared with the pyrolysis of each material separately [10]. A previous study comparable to the present work reported that EZAC accelerated the formation of light-fraction gases and improved the yield and quality of the liquid product [11].

Meanwhile, a study on in-situ and ex-situ catalyst configurations in coffee husk pyrolysis showed that catalyst placement affected both the onset and peak concentration of the target gases, with the ex-situ configuration providing more effective vapor-catalyst contact than the in-situ configuration [12].

However, these prior investigations were strictly limited to evaluating single-component catalyst behaviors. The critical research gap in current literature lies in the unexplored kinetic interactions and reaction selectivity when these two distinct carbonaceous materials are combined into a single mixed catalytic system. Investigating a mixed HRS-EZAC system is scientifically vital because it introduces a potential solid-state synergy between the active mineral components, specifically potassium (K) within the amorphous biomass matrix of HRS, and the high surface-area porous functional groups of EZAC. While the raw amorphous HRS acts as a strong driver for decarboxylation via its alkali metal content, the mature disordered structure of EZAC provides the necessary reactive sites to promote secondary cracking and decarbonylation. Therefore, this work provides a clear novelty by systematically mapping the real-time, second-by-second kinetic profiles of CO and CO_2 formation over this combined mixed matrix under low-temperature isothermal conditions, establishing a mechanistic understanding that has not been addressed by previous single-catalyst studies.

Based on this identified gap, the present study aims to evaluate the kinetic profile of CO and CO_2 formation during PET pyrolysis at 350°C with the addition of HRS, EZAC, and their novel mixture (1:1) as local biomass-based functional carbon materials. Physicochemical characterization data of the materials (FTIR, SEM-EDX, XRD, and TGA-DTA) were integrated with the real-time gas kinetic data to strengthen the mechanistic interpretation of the CO and CO_2 formation patterns governed by each catalyst composition.

2. Methods

2.1 Catalyst Material Preparation

Hibiscus flower powder (*Hibiscus rosa-sinensis*/HRS) was prepared by sun-drying, followed by oven-drying at 55°C for 1 h, grinding with a blender, and sieving through a 200-mesh sieve. Meanwhile Ulin wood activated carbon (*Eusideroxylon zwageri Activated Carbon*/EZAC) was prepared by milling using a rotary ball mill, sieving through a 200-mesh sieve, and chemical activation using 1.5 M NaOH solution for 2 h with magnetic stirring at 200 rpm (carbon-to-NaOH solution ratio of 2.5 g:50 mL), followed by washing with distilled water to pH 6-7 and oven-drying at 105°C for 8 h.

Hibiscus flower powder (*Hibiscus rosa-sinensis*/HRS) and Ulin wood activated carbon (*Eusideroxylon zwageri Activated Carbon*/EZAC) were prepared following the flow shown in the Figure 1.

Alkaline activation of biomass-derived carbon material can release volatile components and yield a porous carbon matrix [13]. The initial characterization results of both individual raw materials (pure HRS and pure EZAC) were adopted from our previous study to serve as a baseline[9], whereas the physicochemical characterizations of the neat PET and the newly developed HRS: EZAC (1:1) mixture were fully generated as original data in the present study.

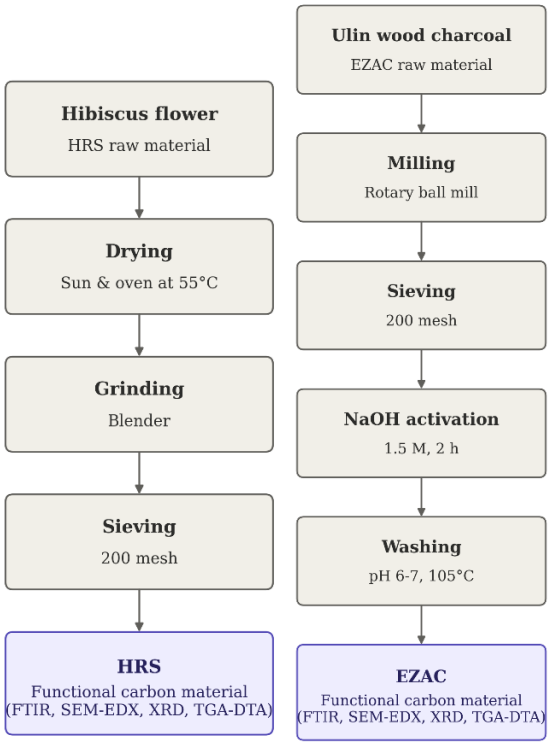


Figure 1. Flow Diagram of The Preparation of Hibiscus Flower Powder (HRS) and Ulin Wood Activated Carbon (EZAC) As Catalyst Materials for PET Pyrolysis

2.2 Pyrolysis Design and Procedure

Pyrolysis was carried out in a stainless-steel batch fixed-bed reactor with a diameter of 20 cm and a height of 15 cm (volume ± 4.7 L). The feedstock consisted of commercial waste PET bottles, obtained from a local supplier, which were manually prepared by cutting them into a uniform size of 1x1 cm.

The reactor was loaded with a total of 500 g of material using an in-situ layering (sandwich) method to optimize the interfacial contact between the polymer and the catalyst particles. Specifically, one handful of the 1x1 cm PET flakes was placed at the bottom of the reactor, followed by scattering a thin, proportional layer of the prepared catalyst powder over it. This alternating process of loading one handful of plastic followed by a layer of catalyst was repeated consistently until the entire feed (475 g PET and 25 g catalyst, maintaining a PET-to-catalyst ratio of 95:5) was fully loaded into the reactor bed. The experimental process flow is shown in Figure 2 below.

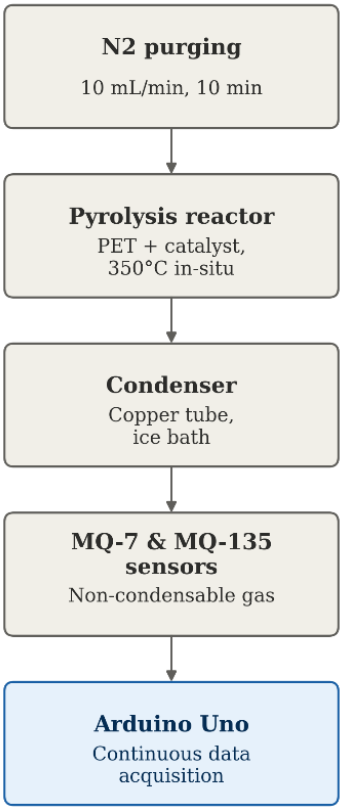


Figure 2. Schematic of the Pyrolysis Reactor System And Non-Condensable Gas Measurement Using MQ-7 And MQ-135 Sensors

The feed mass and fill volume of a batch fixed-bed reactor have been reported to significantly affect the internal temperature profile and pyrolysis product distribution, even exceeding the influence of reactor temperature and reaction time themselves, owing to the limitations of conductive heat transfer from the wall toward the core of the solid bed [14].

Prior to heating, the reactor was purged with N_2 gas (10 mL/min for 10 min) to

provide an inert atmosphere inside the reactor and sweep away any ambient oxygen or gaseous contaminants. The reactor was heated using a Proportional-Integral-Derivative (PID)-controlled LPG stove, from room temperature up to the operating temperature of 350°C, with a type-K thermocouple at the reactor core. The operating temperature of 350°C was set based on TGA-DTA data showing thermal peaks of HRS at 446.80°C and EZAC at 449.55°C, as well as the results of a previous study that also used an operating temperature of 350°C [9,11]. The PID controller regulated the heating profiles with an average heating rate accuracy of approximately ±3.8 °C/min during the temperature ramp-up phase.

The pyrolysis in this study is classified as slow pyrolysis, with a slow heating rate over 5400 s. Crucially, the continuous data logging of CO and CO_2 concentrations was systematically initiated at t = 0 s exactly when the reactor core temperature stabilized at the target set-point of 350°C. While initial polymer softening occurred during the ramp-up stage, tracking the kinetics strictly from the moment of isothermal stabilization ensured a consistent thermal baseline for evaluating and comparing the catalytic performance over the 5400 s reaction period.

Temperature, heating rate, reactor bed height and type, and residence time are recognized as key determinants influencing the yield, product distribution, and the dominance of secondary cracking reactions during pyrolysis [15].

2.3 Gas Measurement System

The pyrolysis gas was passed through a 500-cm copper pipe immersed in an ice bath to condense the condensable products before the non-condensable gas reached the sensors. CO and CO_2 concentrations were measured using MQ-7 and MQ-135 semiconductor sensors integrated with an Arduino Uno microcontroller for continuous data logging from 0 to 5400s, enabling kinetic analysis including the onset time, the concentration rise rate, and the time to reach peak concentration.

Due to the lack of certified pure reference calibration gases in the laboratory, a systematic baseline calibration (zero-point calibration) procedure was implemented to ensure the reliability of the relative trends. The baseline for 0 ppm was established directly in the sensor chamber during the initial 10-minute purging phase, wherein only purity N_2 gas flowed through the system at room temperature before heating commenced. Once a stable flat electrical resistance (R0) baseline was achieved and registered as 0 ppm via the Arduino data logging software, the thermal pyrolysis process was started.

Gas sensors are widely applied to detect various pyrolysis gases and vapors including methane (CH_4), hydrogen (H_2), carbon monoxide (CO), and carbon dioxide (CO_2) to estimate the quality, quantity, and composition of gas products, offering a practical alternative to conventional laboratory-based gas analysis methods for continuous, real-time monitoring [16,17].

However, these semiconductor sensors have inherent limitations, including measurement uncertainty, a tendency for signal drift during extended operations, and potential cross-sensitivity. For instance, while the MQ-135 is primarily targeted for CO_2 detection, it can also exhibit cross-sensitivity toward light volatilized organic fragments and moisture that escape the condenser. Similarly, the MQ-7 sensor can be affected by hydrogen gas variations.

To minimize these measurement uncertainties, the 500-cm copper ice-bath condenser was rigorously maintained to ensure that virtually all heavy and light condensable oil/wax vapors were stripped out, allowing only non-condensable gases to reach the sensor chamber. Consequently, to maintain high scientific rigor, the concentration data obtained in this study are strictly interpreted as indicators of relative kinetic trends (semi-quantitative behavior) rather than absolute analytical concentrations with high precision.

3. Results and Discussion

3.1 Physicochemical Characteristics of the Materials

HRS retained high flavonoid (676.62 mg EQ/100 g) and phenolic (2305.06 mg GAE/100 g) content, supported by FTIR results showing a hydroxyl band (3301.62 cm^{-1}), a conjugated carbonyl band (1651.53 cm^{-1}), and an aromatic ring band (1529.46 cm^{-1}), meanwhile EZAC had a flavonoid content of 166.28 mg EQ/100 g and a phenolic content of 32.04 mg GAE/100 g [9]. It much lower than raw ulin wood (EZ; 470.99 and 2892.48 mg/100 g) that indicating that most organic components were degraded during carbonization and chemical activation, yielding a more porous carbon matrix. FTIR of PET confirmed the ester structure through a carbonyl band (1685.90 cm^{-1}) and C-O bands (1255.16 and 1058.41 cm^{-1}). FTIR of the HRS:EZAC mixture showed a hydroxyl band (3880.37-3277.20 cm^{-1}), an aliphatic C-H band (2954.08 cm^{-1}), aromatic C=C bands (1631.42 and 1549.56 cm^{-1}), and carbonyl/C-O bands (1393.03, 1246.54, and 1039.74 cm^{-1}), a combination of features characteristic of both constituent materials [9].

The EDX analysis is presented in the following Table 1.

Table 1. Elemental composition based on EDX analysis

Component	%C	%O	%Other minerals
HRS	73.68	23.70	K 1.94; Na, Cl, Mg in small amounts
EZ	89.71	10.08	K, Ca, P in small amounts
EZAC	79.28	18.90	Na 1.69 from chemical activation; Si 0.12
HRS:EZAC	84.92	14.56	Na 0.42 from chemical activation; K and Ca in small amounts

EDX analysis showed HRS dominated by C (73.68%) and O (23.70%) with K at 1.94%; EZAC dominated by C (79.28%) and O (18.90%) with residual Na at 1.69% from chemical activation; EZ dominated by C (89.71%) with very low mineral content; and the HRS:EZAC mixture showing an increase in C to 84.92%, a decrease in O to 14.56%, and a sharp decrease in Na to 0.42% that indicating non-uniform mixture homogenization.

Meanwhile XRD showed that HRS, EZ, EZAC, and PET all exhibited an amorphous structure. TGA-DTA showed DTA peaks at 446.80°C (HRS), 351.96°C (EZ), 449.55°C (EZAC), and 435.80°C (PET).

3.2 Kinetic Profile of CO Formation

In the pyrolysis test using the batch fixed-bed reactor at 350°C, the CO gas concentration was detected by the MQ-7 sensor from 0 to 5400 s. The CO concentration versus time is presented in Figure 3.

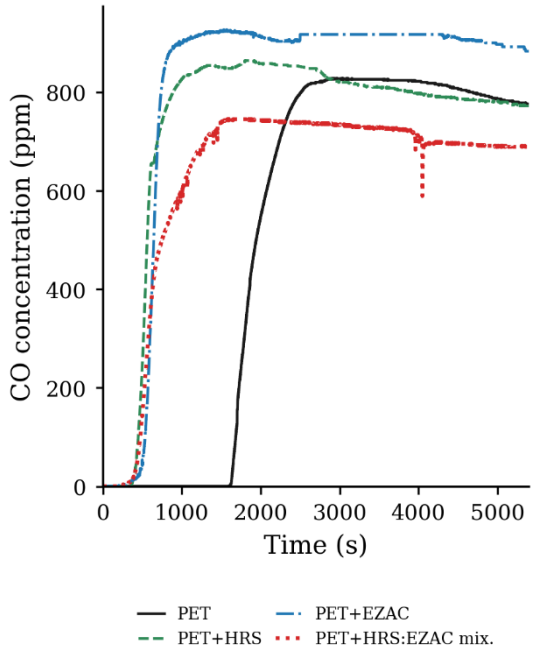


Figure 3. CO concentration versus pyrolysis time for PET, PET+HRS, PET+EZAC, and the PET+HRS:EZAC mixture

Neat PET showed a CO concentration of 0 ppm from 0 s to approximately 1600 s, followed by a gradual and then sharp increase toward the peak after the onset time (1601 s, C-onset 1 ppm) was reached. This is attributable to the nature of the batch fixed-bed reactor, which relies on conductive heat transfer from the wall

toward the core of the solid bed. Without a catalyst, PET decomposition depends heavily on the accumulation of thermal energy propagating through the material before sufficient conversion is reached to produce gas. The highest concentration (C-peak) of 828 ppm was reached at a peak time (t-peak) of 2893 s.

Catalyst addition accelerated PET decomposition into CO gas, as shown by the decrease in onset time compared with catalyst-free PET pyrolysis, presented in Table 2. The same trend was observed for the formation of CO from PET with catalyst, which was reached faster than for PET without catalyst.

A fairly significant decrease in concentration was observed for the PET+HRS: EZAC mixture at around 4000 s, related to substantial terephthalic acid wax formation in the condenser, which caused significant data bias. Although wax formed in all samples, only the PET+HRS: EZAC mixture showed data bias in the CO concentration. This also illustrates that PET pyrolysis still faces the challenge of wax formation in the condenser, with the HRS: EZAC mixture producing the greatest amount of wax.

The CO formation rate from the pyrolysis results can be calculated using the following equation:

$$r_{CO} = \frac{dC_{CO}}{dt} = \frac{C\ peak - C\ onset}{t\ peak - t\ onset} \quad (1)$$

The CO concentration rise rate data are presented in Table 2.

Table 2. CO concentration rise rate

Component	C-onset (ppm)	t-onset (s)	C-peak (ppm)	t-peak (s)	r_{CO} (ppm/s)
PET	1	1601	828	2893	0.640
PET+HRS	2	357	864	1799	0.598
PET+EZAC	2	203	927	1534	0.695
PET+ HRS:EZAC mixture	2	231	745	1571	0.554

PET+EZAC showed the highest values across the four measured CO kinetic parameters simultaneously (fastest onset time, highest formation rate, shortest time to peak, and highest peak concentration) among the catalyzed compositions, indicating that EZAC selectively accelerates the decarbonylation pathway**.** This behavior suggests that EZAC likely plays a major role in lowering the initial energy barrier for the decarbonylation pathway, potentially enhancing both the initiation speed and reaction intensity under the tested conditions.

Interestingly, neat PET showed the rise rate closest to that of PET+EZAC despite its much slower onset, indicating that the role of the catalyst in CO formation is more dominant in lowering the initial energy barrier, or activation energy, than in altering the reaction rate once the reaction is underway. Diverse oxygen-containing functional groups on the activated carbon surface play a key role in determining catalytic activity and selectivity [6], while its high surface area and reactive sites facilitate contact with volatile compounds, supporting secondary cracking and decarbonylation reactions [7].

3.3 Kinetic Profile of CO_2 Formation

CO_2 gas formed during pyrolysis was detected by the MQ-135 sensor from 0 to 5400 s. Neat PET showed a CO_2 concentration of 0 ppm from 0 s to approximately 1600 s, followed by a gradual and then sharp increase toward the peak after the onset time (1672 s, C-onset 2 ppm) was reached. The highest concentration (C-peak) of 608 ppm was reached at a peak time (t-peak) of 3919 s. Catalyst addition accelerated PET decomposition into CO_2 gas, as shown by the decrease in onset time compared with catalyst-free PET pyrolysis, presented in Table 3.

A fairly significant anomaly was observed in the concentration data for the PET+HRS: EZAC mixture, although an increase continued until the end of the pyrolysis period. This is likely related to the substantial amount of terephthalic acid in the condenser. Although wax formed in all samples, only the PET+HRS: EZAC

mixture showed the largest bias in the CO2 concentration data. Another possible cause is the homogeneity of the HRS:EZAC mixture with PET, resulting in non-uniform CO_2 production.

The CO_2 formation rate from the pyrolysis results can be calculated using the following equation:

$$r_{CO2} = \frac{dC_{CO2}}{dt} = \frac{C\ peak - C\ onset}{t\ peak - t\ onset} \quad (2)$$

The CO_2 concentration versus time is presented in Figure 4.

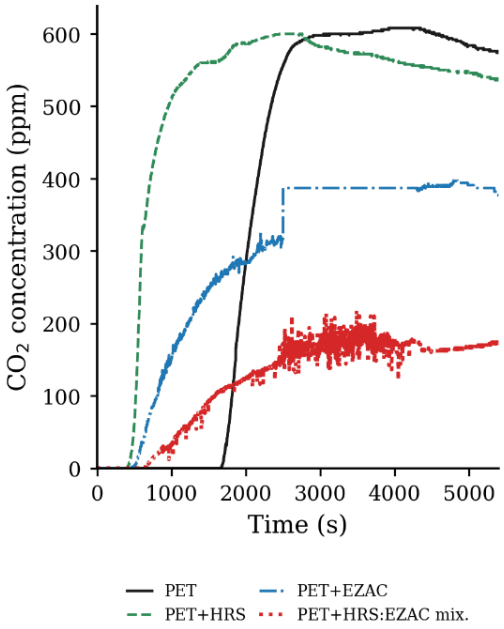


Figure 4. CO_2 concentration versus pyrolysis time for PET, PET+HRS, PET+EZAC, and the PET+HRS: EZAC mixture

The CO_2 concentration rise rate data are presented in Table 3.

Table 3. CO_2 concentration rise rate

Component	C-onset (ppm)	t-onset (s)	C-peak (ppm)	t-peak (s)	r_{CO2} (ppm/s)
PET	2	1672	608	3919	0.270
PET+HRS	2	412	600	2451	0.293
PET+EZAC	2	471	397	4790	0.091
PET+ HRS:EZAC mixture	2	649	218	3489	0.076

PET+HRS showed the best performance across three parameters simultaneously: fastest onset time, highest rate, and fastest time to reach peak concentration, while neat PET closely competed for the highest peak concentration.

Alkali and alkaline earth metals in biomass are known to accelerate the initial stage of decomposition and affect the cleavage of carboxyl and carbonyl groups, promoting the decarboxylation reaction [4]. Potassium in particular has been reported to play an active role in this pathway through its interaction with biomass components during pyrolysis [5].

This pathway is highly consistent with the detected potassium (K) content in the HRS sample, which supports the hypothesis that the functional carbon groups in HRS may actively assist the decarboxylation process during the active thermal degradation phase, rather than merely accelerating the initial reaction onset.

3.4 Reaction Pathway Selectivity: Comparison of CO and CO_2

The comparison between CO and CO_2 across two kinetic parameters, namely peak concentration and formation rise rate, is presented in the following Figures 5 and 6.

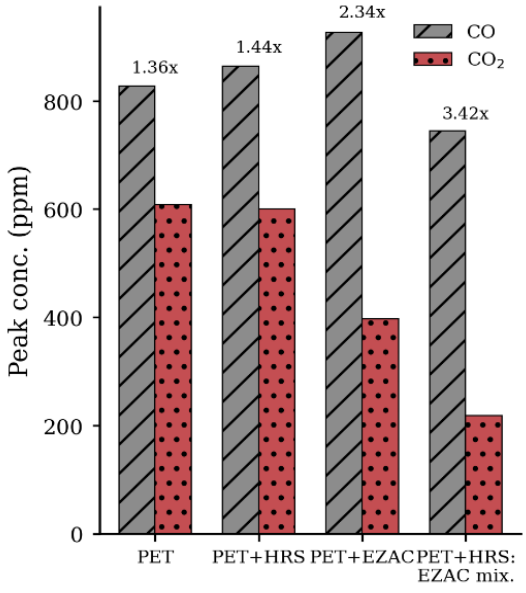


Figure 5. Comparison of CO and CO_2 peak concentration formed during pyrolysis

The CO/CO_2 ratio based on peak concentration was 1.36 (PET), 1.44

(PET+HRS), 2.34 (PET+EZAC), and 3.42 (PET+mixture).

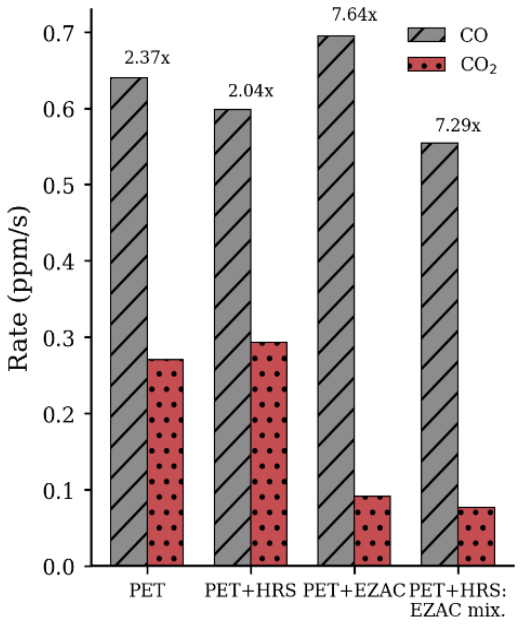


Figure 6. Comparison of CO and CO_2 formation rise rate during pyrolysis

The ratio based on rise rate was 2.37 (PET), 2.04 (PET+HRS), 7.64 (PET+EZAC), and 7.29 (PET+mixture) (Figure 6).

HRS was the only sample with a lower rate ratio than neat PET, indicating that HRS promotes CO_2 proportionally more than CO. In contrast, EZAC and the mixture showed a rate ratio more than three times that of neat PET, confirming a strong shift toward decarbonylation. This pattern is consistent with DFT-based mechanistic studies showing that CO_2 is formed through decarboxylation during the early stage, whereas CO is formed through radical decarbonylation during the secondary stage [3].

3.5 Relationship Between Characterization and Catalytic Performance

The potassium (K) content found in HRS, alongside its predominantly amorphous matrix, offers a plausible structural basis to explain its accelerated CO_2 rise rate. The amorphous structure could potentially provide greater accessibility for organic components and potassium (K) to interact continuously with PET volatiles, thereby appearing to support decarboxylation [4,5]. In EZAC, the combination of oxygen-containing groups, residual Na, and disordered carbon structure is highly compatible with its observed role in facilitating secondary reactions and potentially directing the reaction selectivity toward decarbonylation [6,7].

The mixed sample showed a non-additive suppression of both gases' kinetics compared with the single catalysts. SEM imaging showed HRS particles attached to the EZAC surface, supporting the possibility of a genuine chemical interaction. However, EDX showed Na in the mixture (0.42%) much lower than in EZAC alone (1.69%), more likely attributable to non-uniform mixing homogenization, reinforced by the greatest wax formation and highest CO_2 signal fluctuation observed in this sample. These three lines of evidence point to two parallel, as yet unresolved hypotheses: an antagonistic chemical interaction between active sites, or heterogeneous catalyst distribution within the in-situ system.

3.6 Implications for Process Sustainability

The utilization of HRS and EZAC as local biomass-waste-based functional carbon materials is in line with the circular economy principle that promotes resource efficiency [8].

Temperature, heating rate, reactor bed height and type, and residence time are key determinants influencing the yield and product distribution of pyrolysis [15], so the accelerated onset observed for all catalyzed samples compared with neat PET at a constant temperature indicates a potential process efficiency that could be further examined through a Life Cycle Assessment. Both CO and CO_2 represent environmental burdens generated by the pyrolysis process that need to be managed, regardless of their potential utilization.

4. Conclusion

In conclusion, the evaluation of local biomass-based functional carbon materials from HRS, EZAC, and their mixture during PET pyrolysis at 350°C consistently demonstrated an accelerated reaction onset compared with catalyst-free PET. As confirmed findings, the single-catalyst systems exhibited distinct selectivities; the addition of EZAC outperformed the other samples across all CO kinetic parameters, achieving the fastest onset time of 203 s and a peak concentration of 927 ppm. Conversely, the raw HRS outperformed the other samples in the CO_2 formation rate, reaching a rate of 0.294 ppm/s and a peak concentration of 600 ppm.

Regarding the catalytic mechanisms, the available characterization and gas trend data suggest two parallel hypotheses to explain the observed non-additive kinetic suppression in the mixed HRS-EZAC sample: either an antagonistic chemical interaction between the active alkali metal sites and porous functional groups, or a heterogeneous physical catalyst distribution arising from the manual in-situ layering process. Because these mechanistic pathways remain as unverified hypotheses within the scope of this study, further research is highly recommended to validate these interactions. Future work should focus on utilizing an ex-situ dual-bed reactor configuration to isolate vapor-catalyst contact, performing localized SEM-EDX elemental mapping to quantify mixing uniformity, and conducting a comprehensive Life Cycle Assessment (LCA) to evaluate the environmental sustainability of these functional carbon materials.

Acknowledgements

The authors thank the following laboratories for their support in the completion of this project: (1) Integrated Laboratory, Universitas Islam Malang; (2) Internal Combustion Engine Laboratory, Department of Mechanical Engineering, Faculty of Engineering, Universitas Brawijaya; (3) Integrated Laboratory, Faculty of Agricultural Technology, Universitas Brawijaya; and (4) Integrated Research Laboratory, Universitas Brawijaya (LRT-UB).

REFERENCES

[1]. Enache, A.C. et al., 2024. Polyethylene Terephthalate (PET) Recycled by Catalytic Glycolysis: A Bridge toward Circular Economy Principles. Materials, 17(12), 2991. DOI: 10.3390/ma17122991

[2]. Alotaibi, M. and Williams, P.T., 2026. Methane Production from the Three-Stage (i) Pyrolysis (ii) Catalytic Cracking (iii) Catalytic Hydrogenation of Polyethylene Terephthalate (PET) Plastic Waste. Waste Biomass Valorization. DOI: 10.1007/s12649-026-03712-x

[3]. Huang, J.B. et al., 2022. Insights into the thermal degradation mechanisms of polyethylene terephthalate dimer using DFT method. Chemosphere, 291, 133112. DOI: 10.1016/j.chemosphere.2021.133112

[4]. Wang, W. et al., 2022. Review on the catalytic effects of alkali and alkaline earth metals (AAEMs) including sodium, potassium, calcium and magnesium on the pyrolysis of lignocellulosic biomass and on the co-pyrolysis of coal with biomass. J Anal Appl Pyrolysis, 163, 105479. DOI: 10.1016/j.jaap.2022.105479

[5]. Fan, H. et al., 2021. Effect of potassium on the pyrolysis of biomass components: Pyrolysis behaviors, product distribution and kinetic characteristics. Waste Management, 121, 255–64. DOI: 10.1016/j.wasman.2020.12.023

[6]. Liu, X. et al., 2026. Research and Perspectives on Surface Functional Group Characterization of Activated Carbon Catalysts. Catalysts, 16(6), 558. DOI: 10.3390/catal16060558

[7]. Choi, M.J. et al., 2021. Air gasification of polyethylene terephthalate using a two-stage gasifier with active carbon for the production of H_2 and CO. Energy 223(C), 120122. DOI: 10.1016/j.energy.2021.120122

[8]. Nazarloo, N.H. et al. 2024. Catalytic pyrolysis of plastic waste using activated carbon from cotton waste. J Anal Appl Pyrolysis, 182(6515), 106692. DOI: 10.1016/j.jaap.2024.106692

[9]. Sartika, G. et al., 2026. Sintesis dan Karakterisasi Bunga Sepatu dan Karbon Kayu Ulin Untuk Katalis Pada Proses Pirolisis Sampah Plastik. TURBO: Jurnal Program Studi Teknik Mesin, 15(2), 1–11. DOI: 10.24127/trb.v15i2.5363

[10]. Yani, A. et al., 2025. Trash to Treasure: Co-Pyrolysis of PET Plastic and Hibiscus Rosa-Sinensis for Sustainable Syngas Production. Proceedings of the 10th International Conference and Exhibition on Sustainable Energy and Advanced Materials, 61–75. DOI:10.1007/978-981-96-5063-7_6

[11]. Yani, A et al., 2026. Enhancing pyrolysis oil yield and quality via low-temperature catalytic pyrolysis of pet waste over activated carbon derived from euxideroxylon zwageri. Mechanical Engineering for Society and Industry, 6(2), 415-440. DOI: 10.31603/mesi.16415

[12]. Irawan, D. et,al., 2026. The role of zeolite catalysts on methane and hydrogen production using in-situ and ex-situ methods in biomass pyrolysis. Chemical Review and Letters, 9(5), 1076-1086. DOI: 10.22034/crl.2026.583247.1902

[13]. Alcañiz-Monge, J. et al., 2022. Chemical Activation of Lignocellulosic Precursors and Residues: What Else to Consider?. Molecules, 27(5), 1630. DOI: 10.3390/molecules27051630

[14]. Papuga, S. et al., 2024. Effect of Feed Mass, Reactor Temperature, and Time on the Yield of Waste Polypropylene Pyrolysis Oil Produced via a Fixed-Bed Reactor. Polymers, 16(10), 1302. DOI: 10.3390/polym16101302

[15]. Al-Rumaihi, A. et al., 2022. A review of pyrolysis technologies and feedstock: A blending approach for plastic and biomass towards optimum biochar yield. Renewable and Sustainable Energy Reviews, 167, 112715. DOI: 10.1016/j.rser.2022.112715

[16]. Nagahage, I.S.P. et al., 2021. Assessment of the applicability of a low-cost sensor–based methane monitoring system for continuous multi-channel sampling. Environmental Monitoring Assessment, 193, 509. DOI: 10.1007/s10661-021-09290-w

[17]. Zhang, H. et al., 2022. A review of sensor applications towards precise control of pyrolysis of solid waste and biomasses. Renewable and Sustainable Energy Reviews, 169, 112915. DOI: 10.1016/j.rser.2022.112915